ELSEVIER

Carbohydrate Research 337 (2002) 1861–1871

CARBOHYDRATE RESEARCH

www.elsevier.com/locate/carres

Disaccharide conformational maps: 3D contours or 2D plots?☆

Carlos A. Stortz,* Alberto S. Cerezo

Departamento de Química Orgánica-CIHIDECAR, Facultad de Ciencias Exactas y Naturales, Universidad de Buenos Aires, Ciudad Universitaria, 1428 Buenos Aires, Argentina

Received 21 June 2002; accepted 29 July 2002

Abstract

The potential energy surfaces of several α-(1→3)- and β-(1→4)-linked disaccharides were obtained and plotted in terms of energy versus ψ glycosidic angle. These plots were compared to those obtained previously in the way of the usual 3D contour maps, which relate the energy with the two glycosidic angles (ϕ and ψ). Given the usually small variations of the ϕ angle in the low-energy regions (at least using MM3), both kinds of graphs lead to similar conclusions concerning flexibility measurements by two different methods and assessment of the effects of sulfation and/or hydroxyl group orientation. Only second-order effects were found with some sulfated disaccharides, not changing the general conclusions. The computational efforts required to produce those plots are smaller, and the plots are easier to interpret. Besides, the conversion of a 3D map into a 2D plot leaves the possibility of constructing 3D maps of carbohydrates including a second variable different to ϕ, e.g., the second ψ angle of a trisaccharide or the ω angle of a 6-linked disaccharide.

Keywords: Disaccharides; Conformational analysis; Molecular mechanics; MM3; Ramachandran map

1. Introduction

Conformational analysis of disaccharides is usually accompanied by the generation of a Ramachandran-like 3D contour map as a tool in understanding their conformational features[1–3] and predicting the likelihood of different molecular conformations.[4] In these maps the energy is determined for all mutual orientations of the monosaccharide residues expressed by the glycosidic angles ϕ and ψ. First studies were carried out by rigid residue analysis,[3] but, by 1979, flexible residue analysis was initiated by allowing all variables to relax.[5–7] From the late 1980s on, many disaccharides were modeled using different force fields (and even QM methods), and the results were expressed with 3D contour maps.[4,8–17] The map is actually an adiabatic representation of the true conformational hypersurface that depends not only on the glycosidic angles but also on many other variables, among them the orientation of secondary hydroxyl groups and hydroxymethyl groups, the different degrees of puckering of the rings, etc., which might complicate reaching true adiabaticity.[18] However, it is usually considered that the most important energy variations are those related with the glycosidic angles ϕ and ψ, and thus, the 3D contour adiabatic map against these two variables is the usual output of disaccharide conformational analysis.

When looking at the maps, particularly those produced with MM3 (one of the force fields considered to be more reliable for carbohydrates),[14–23] the conclusions drawn from these maps are that (especially for α-linked disaccharides) 'a trough centered at a more or less fixed ϕ angle is observed, and it contains the main minima, each of which exhibits a clearly different ψ angle'.[14,20] This ϕ angle matches that expected as an expression of the *exo*-anomeric effect, although it is doubtful if it occurs solely on grounds of this effect, as it has been shown that other force fields (as MM2) with a weaker parameterization of this effect, also give rise to similar maps,[19,24] and *C*-disaccharides, for which *exo*-anomeric effect cannot occur, also exhibit similar angles.[25,26] A similar behavior for the ϕ angle was found in X-ray crystallographic analysis of different disaccharides and derivatives.[27]

☆ Throughout this paper, '3D contours' indicate traditional Ramachandran contour maps, while '2D plots' indicate x–y graphs representing energy versus a single angle.

* Corresponding author. Tel./fax: +54-11-4576-3346
E-mail address: stortz@qo.fcen.uba.ar (C.A. Stortz).

0008-6215/02/$ - see front matter
PII: S0008-6215(02)00257-4

The presence of two glycosidic angles, one which varies only slightly, and the other which varies strongly in the main minima leads to the title question. Is it worth it to do a 3D contour map, or can a regular x–y plot also explain the main conformational features of a disaccharide? Herein is presented a comparison of the methods when working on several α-(1→3)- or β-(1→4)-linked disaccharides that have been previously studied.[20–23]

2. Methods

The molecular mechanics program MM3 (92) (QCPE, Indiana University, USA), developed by Allinger and co-workers, was used.[28,29] However, the MM3 routines were modified as suggested[30] by changing the maximum atomic movement from 0.25 to 0.10 Å. The dihedral angles ϕ and ψ are defined by atoms O-5′–C-1′–O-n–C-n and C-n + 1–C-n–O-n–C-1′, respectively, while ϕ_H and ψ_H are defined by atoms H-1′–C-1′–O-n–C-n and H-n–C-n–O-n–C-1′, respectively. It has been suggested[31] that torsion angles should be driven in terms of non-hydrogen atoms, given the different motions of the three atoms during driven rotation and the inaccuracy of hydrogen atom positions in diffraction studies. However, in order to keep up with our previous studies, some calculations were driven in terms of hydrogen atoms.

For sulfated disaccharides, MM3 parameters for the sulfate group were taken from Lamba et al.,[32] and a dielectric constant of 3.0 was used. In that model, the charge on the sulfate groups is emulated by S–O bond dipoles. No cations were added. Some of the non-sulfated disaccharides were also studied at a dielectric constant of 80, where the electrostatic and hydrogen bond interactions were completely damped.[18] The 2D plots were generated using the previous 3D data.[18–23] To generate each plot, for each compound, the 20–30 conformers found[18–23] with ϕ values near to those expected by the *exo*-anomeric effect (main well), and different ψ values and varied exocyclic groups orientations were chosen as starting points. Minimization (with a restrained ψ or ψ_H varied in 20° intervals) was carried out by the block diagonal Newton–Raphson procedure, using both the dihedral drivers 2 (sequential minimization) and 4 (minimization from the starting point). The rest of the variables were allowed to relax. The optimization was terminated when the decrease in energy converged to a value lower than 2 cal/mol. The energy for each point was the lowest of any of the 40–50 calculations. In this way, only the conformation of minimal energy for each ψ value was recorded, thus giving rise to 2D conformational adiabatic plots as function of the ψ angle.

The absolute flexibility for 3D and 2D plots was calculated as described by Koca et al.[33,34] First, the energies and geometries of the transition states between minimum energy regions were calculated: they were first estimated from the walk within the adiabatic maps, and then determined by a full-matrix analysis, confirming that only one negative eigenvalue appeared. When more than one transition state was present in the same region, the one with lower energy was considered. Then, the 3D absolute flexibility[22,23,32,33] $\Phi_{\phi,\psi}$ was calculated as:

$$\Phi_{\phi,\psi} = \sum_{i=1}^{n}\left(\frac{e^{-Ei/RT}}{\sum_{k=1}^{n} e^{-Ek/RT}}\right) \times \left[\sum_{j=1}^{m}(e^{-(E_j - E_{gm})/RT}) \times \left(\frac{|\phi_i - \phi_j| + |\psi_i - \psi_j|}{720}\right)\right]$$

while the 2D absolute flexibility was calculated as:

$$\Phi_{\psi} = \sum_{i=1}^{n}\left(\frac{e^{-Ei/RT}}{\sum e^{-Ek/RT}}\right) \times \left[\sum_{j=1}^{m}(e^{-(E_j - E_{gm})/RT}) \times \left(\frac{|\psi_i - \psi_j|}{360}\right)\right]$$

where E_{gm} is the energy of the global minimum, n is the number of minima (indexes i and k), m the number of transition states (index j) surrounding minimum i, the ϕ, ψ angles are given in degrees, R is the universal gas constant and T the temperature (set to 25 °C = 298.16 K).

The partition functions were calculated as:[21]

$$q_{\phi,\psi} = \Delta\phi \times \Delta\psi \times \sum_{i=1}^{324} e^{-(E_i - E_{gm})/RT}$$

$$q_{\psi} = \Delta\psi \times \sum_{i=1}^{18} e^{-(E_i - E_{gm})/RT}$$

where $\Delta\phi$ and $\Delta\psi$ are the grid spacings (20° each in this case) and the summation is carried out over the entire surface (324 points for ϕ,ψ maps, 18 points for ψ plots). French and co-workers[4] used the name 'probability volume' for this function.

3. Results and discussion

The 3D contour maps of several α-(1→3)- and β-(1→4)-linked disaccharides and analogs were analyzed previously.[18–23] Herein, these analyses were carried out relating the energy of each conformation with the ψ angle, while allowing the ϕ angle to relax, since ϕ usually falls in a narrow range of values in the low-energy regions. Table 1 lists the disaccharides which were

Table 1
The compounds under study in this work

Compd[a]		Non reducing unit	Linkage	Reducing unit
1	ax,eq	4,6-dideoxy-α-D-*xylo*-hexopyranosyl	1→3	6-deoxy-β-D-glucopyranose
2	ax,eq	4,6-dideoxy-α-D-*xylo*-hexopyranosyl	1→3	6-deoxy-β-D-galactopyranose
3	ax,eq	4,6-dideoxy-α-D-*xylo*-hexopyranosyl	1→3	6-deoxy-β-D-mannopyranose
4	ax,eq	4,6-dideoxy-α-D-*xylo*-hexopyranosyl	1→3	6-deoxy-β-D-talopyranose
5	ax,eq	4,6-dideoxy-α-D-*lyxo*-hexopyranosyl	1→3	6-deoxy-β-D-glucopyranose
6	ax,eq	4,6-dideoxy-α-D-*lyxo*-hexopyranosyl	1→3	6-deoxy-β-D-galactopyranose
7	ax,eq	4,6-dideoxy-α-D-*lyxo*-hexopyranosyl	1→3	6-deoxy-β-D-mannopyranose
8	ax,eq	4,6-dideoxy-α-D-*lyxo*-hexopyranosyl	1→3	6-deoxy-β-D-talopyranose
9	ax,ax	4,6-dideoxy-α-D-*xylo*-hexopyranosyl	1→3	6-deoxy-β-D-allopyranose
10	ax,ax	4,6-dideoxy-α-D-*xylo*-hexopyranosyl	1→3	6-deoxy-β-D-gulopyranose
11	ax,ax	4,6-dideoxy-α-D-*xylo*-hexopyranosyl	1→3	6-deoxy-β-D-altropyranose
12	ax,ax	4,6-dideoxy-α-D-*xylo*-hexopyranosyl	1→3	6-deoxy-β-D-idopyranose
13	ax,ax	4,6-dideoxy-α-D-*lyxo*-hexopyranosyl	1→3	6-deoxy-β-D-allopyranose
14	ax,ax	4,6-dideoxy-α-D-*lyxo*-hexopyranosyl	1→3	6-deoxy-β-D-gulopyranose
15	ax,ax	4,6-dideoxy-α-D-*lyxo*-hexopyranosyl	1→3	6-deoxy-β-D-altropyranose
16	ax,ax	4,6-dideoxy-α-D-*lyxo*-hexopyranosyl	1→3	6-deoxy-β-D-idopyranose
1′	eq,eq	3,6-anhydro-α-D-galactopyranosyl	1→3	β-D-galactopyranose
2′	eq,eq	3,6-anhydro-2-sulfonato-α-D-Gal*p*	1→3	β-D-galactopyranose
3′	eq,eq	3,6-anhydro-α-D-galactopyranosyl	1→3	β-D-galactopyranose 2-sulfate
4′	eq,eq	3,6-anhydro-2-sulfonato-α-D-Gal*p*	1→3	β-D-galactopyranose 2-sulfate
5′	eq,eq	3,6-anhydro-α-D-galactopyranosyl	1→3	β-D-galactopyranose 4-sulfate
6′	eq,eq	3,6-anhydro-2-sulfonato-α-D-Gal*p*	1→3	β-D-galactopyranose 4-sulfate
7′	eq,eq	3,6-Anhydro-α-D-galactopyranosyl	1→3	β-D-galactopyranose 2,4-disulfate
8′	eq,eq	3,6-Anhydro-2-sulfonato-α-D-Gal*p*	1→3	β-D-galactopyranose 2,4-disulfate
9′	eq,eq	3,6-anhydro-α-D-galactopyranosyl	1→3	4,6-*O*-(1-carboxylethylidene)-β-D-Gal*p*
10′	eq,eq	3,6-anhydro-2-sulfonato-α-D-Gal*p*	1→3	4,6-*O*-(1-carboxylethylidene)-β-D-Gal*p*
1″	ax,eq	α-D-galactopyranosyl	1→3	β-D-galactopyranose
2″	ax,eq	α-D-galactopyranosyl	1→3	β-D-galactopyranose 2-sulfate
3″	ax,eq	α-D-galactopyranosyl	1→3	β-D-galactopyranose 4-sulfate
4″	ax,eq	2-sulfonato-α-D-galactopyranosyl	1→3	β-D-galactopyranose 2-sulfate
5″	ax,eq	2-sulfonato-α-D-galactopyranosyl	1→3	β-D-galactopyranose 4-sulfate
6″	ax,eq	6-sulfonato-α-D-galactopyranosyl	1→3	β-D-galactopyranose 2-sulfate
7″	ax,eq	6-sulfonato-α-D-galactopyranosyl	1→3	β-D-galactopyranose 4-sulfate
8″	ax,eq	2,6-disulfonato-α-D-Gal*p*	1→3	β-D-galactopyranose 2-sulfate
9″	ax,eq	2,6-disulfonato-α-D-Gal*p*	1→3	β-D-galactopyranose 4-sulfate
1b	eq,ax	β-D-galactopyranosyl	1→4	α-D-galactopyranose
2b	eq,ax	2-sulfonato-β-D-galactopyranosyl	1→4	α-D-galactopyranose
3b	eq,ax	4-sulfonato-β-D-galactopyranosyl	1→4	α-D-galactopyranose
4b	eq,ax	2-sulfonato-β-D-galactopyranosyl	1→4	α-D-galactopyranose 2-sulfate
5b	eq,ax	4-sulfonato-β-D-galactopyranosyl	1→4	α-D-galactopyranose 2-sulfate
6b	eq,ax	2-sulfonato-β-D-galactopyranosyl	1→4	α-D-galactopyranose 6-sulfate
7b	eq,ax	4-sulfonato-β-D-galactopyranosyl	1→4	α-D-galactopyranose 6-sulfate
8b	eq,ax	2-sulfonato-β-D-galactopyranosyl	1→4	α-D-galactopyranose 2,6-disulfate
9b	eq,ax	4-sulfonato-β-D-galactopyranosyl	1→4	α-D-galactopyranose 2,6-disulfate
10b	eq,eq	β-D-galactopyranosyl	1→4	3,6-anhydro-α-D-galactopyranose
11b	eq,eq	2-sulfonato-β-D-galactopyranosyl	1→4	3,6-anhydro-α-D-galactopyranose
12b	eq,eq	4-sulfonato-β-D-galactopyranosyl	1→4	3,6-anhydro-α-D-galactopyranose
13b	eq,eq	β-D-galactopyranosyl	1→4	3,6-anhydro-α-D-Gal*p* 2-sulfate
14b	eq,eq	2-sulfonato-β-D-galactopyranosyl	1→4	3,6-anhydro-α-D-Gal*p* 2-sulfate
15b	eq,eq	4-sulfonato-β-D-galactopyranosyl	1→4	3,6-anhydro-α-D-Gal*p* 2-sulfate

[a] Compounds **17** and **18** are 4-(tetrahydropyran-2-yloxy)tetrahydropyrane with axial–equatorial and axial–axial linkages, respectively, while **20** is (*R*)-1-isopropoxyethanol. The acronym for the compounds is followed by an indication of the type of linkage (ax = axial, eq = equatorial).

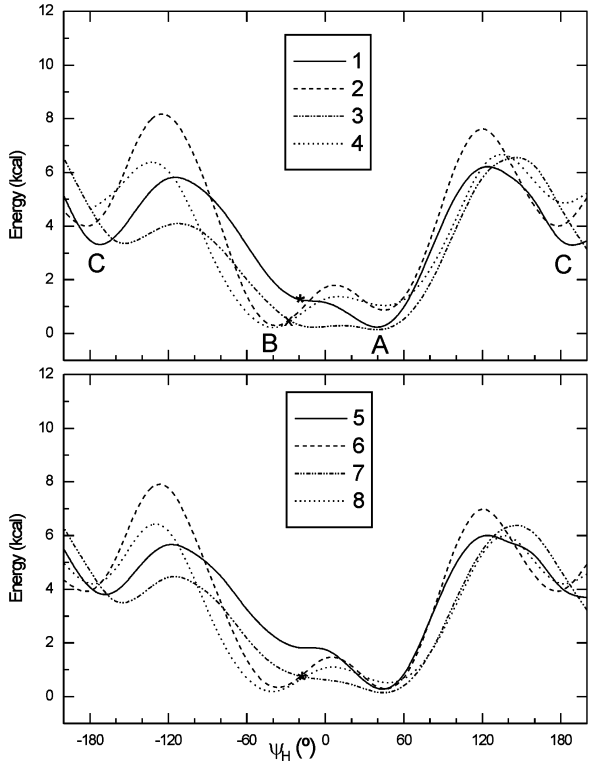

Fig. 1. Relaxed MM3 surface (2D plot) for compounds **1**–**8** ($\varepsilon = 3$). The symbols indicate the positions of reported crystal structures[35–37] with the configuration of **1** (*), **2** (×) and **7** (*).

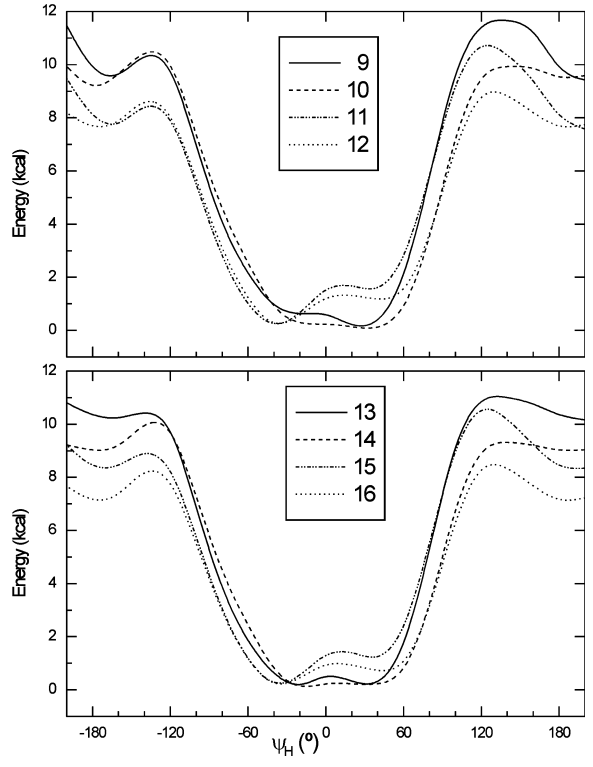

Fig. 2. Relaxed MM3 surface (2D plot) for compounds **9**–**16** ($\varepsilon = 3$).

analyzed, grouped in four blocks: 3-*O*-(4,6-dideoxy-α-hexopyranosyl)-6-deoxy-β-hexopyranoses and analogs,[22] 3-*O*-(3,6-anhydro-α-D-galactopyranosyl)-β-D-galactopyranose and sulfated derivatives,[21] 3-*O*-(α-D-galactopyranosyl)-β-D-galactopyranose and sulfated derivatives,[18–20] and finally their equivalent disaccharides with reverse linkage, i.e., 4-*O*-(β-D-galactopyranosyl)-α-D-galactopyranose, plus its 3,6-anhydro and sulfated derivatives.[23] The corresponding potential energy plots are shown in Fig. 1 (compounds **1**–**8**), Fig. 2 (compounds **9**–**16**), Fig. 3 (compounds **17**, **18** and **20**), Fig. 4 (compounds **1′**–**10′**), Fig. 5 (compounds **1″**–**9″**), Fig. 6 (compounds **1b**–**9b**) and Fig. 7 (compounds **10b**–**15b**). Fig. 1 shows the labels for the three minima present in all graphs, i.e., those labelled as **A**, **B** and **C**, carrying ψ_H values in g^+, g^- and t arrangement, respectively. The figures show a low energy **A**–**B** region for all the compounds under study.

Comparison of the 3D and 2D plots.—In order to monitor the feasibility of depicting the conformational features of a disaccharide from a 2D plot (energy versus ψ angle), the flexibility measurements calculated for the 3D maps[22,23] were completed for the other compounds and accompanied by the same calculations on the 2D plots. The flexibility, measured both as a partition function and as an absolute flexibility, is shown in Table 2 (compounds **1**–**20**), Table 3 (compounds **1′**–**10′** and **1″**–**9″**), and Table 4 (compounds **1b**–**15b**). In order to control the statistical validity of the calculation of q_ψ (provided that only few points define its value), the calculation was repeated using a 5° grid for compounds **1**, **5′** and **2b**, yielding the same results (less than 1% difference).

Flexibility measured by the partition function. For the partition function, a molecule with no flexibility at all in the ϕ direction should show a ratio of $q_{\phi,\psi}$:q_ψ equal to 20° (i.e., the ϕ grid dimension, see Section 2). On the other hand, if the molecule is completely flexible in the ϕ direction (i.e., shows the same value of energy for all ϕ values for each ψ value), this ratio should be 360°. The study for compounds **1**–**20** (Table 2) at either dielectric constant, as well as those for the carrageenan disaccharides carrying 3,6-anhydrogalactose (**1′**–**10′**, Table 3, and **10b**–**15b**, Table 4) shows that the $q_{\phi,\psi}$:q_ψ ratios have magnitudes between 21 and 36, which is very close to the limiting value of 20, thus confirming the restriction in ϕ values observed in those maps. Fig. 8 shows that a fair linear correlation can be made between $q_{\phi,\psi}$ and q_ψ. However, a further observation of the results (Tables 2–4) suggests that the $q_{\phi,\psi}$:q_ψ ratio may increase for high values of the partition function, indicating a slight deviation from linearity. For the carrageenan disaccharides (not carrying 3,6-anhydrogalactose), a clear influence of the sulfation pattern of the β-D-galactose unit is observed (Tables 3 and 4): for α-linked disaccharides those sulfated on C-4 (**3″**, **5″**, **7″**

and **9**″) exhibit lower $q_{\phi,\psi}$:q_{ψ} ratios (20–23, Table 3), while 2-sulfated compounds (**2**″, **4**″, **6**″ and **8**″) give much higher values (29–36, unshaded diamonds on Fig. 8), and the non-sulfated one yields an in-between value (**1**″, 26). A similar effect, but reversed, is observed for β-linked disaccharides: those sulfated on C-2 of the β unit (**2b**, **4b**, **6b** and **8b**) show low $q_{\phi,\psi}$:q_{ψ} ratios (23–28, Table 4), while those compounds not sulfated

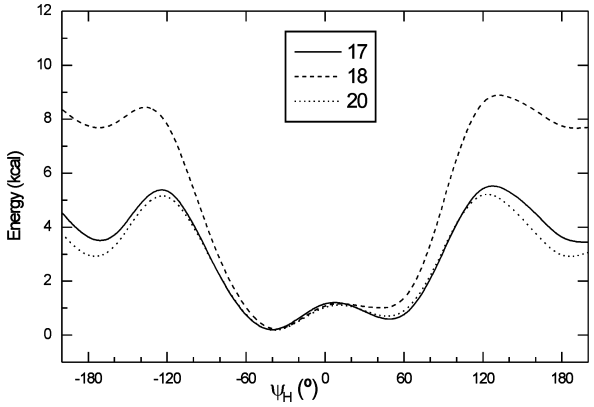

Fig. 3. Relaxed MM3 surface (2D plot) for compounds **17**, **18** and **20** ($\varepsilon = 3$).

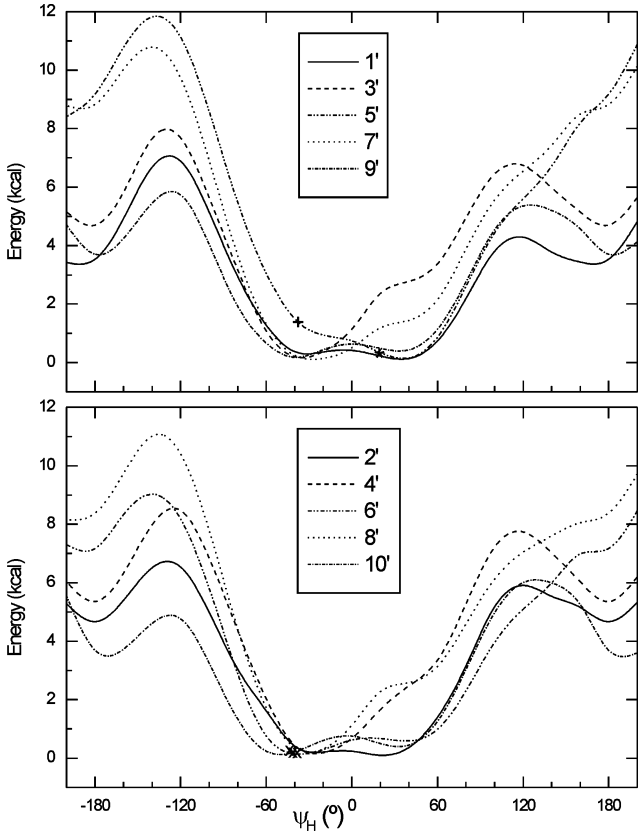

Fig. 4. Relaxed MM3 surface (2D plot) for compounds **1**′–**10**′. The symbols indicate the positions of a published crystal structure[38] of **1**′ (*), and of fiber diffraction studies of carrageenans with repeating units **5**′ (+),[39] and **6**′ (×).[39–42]

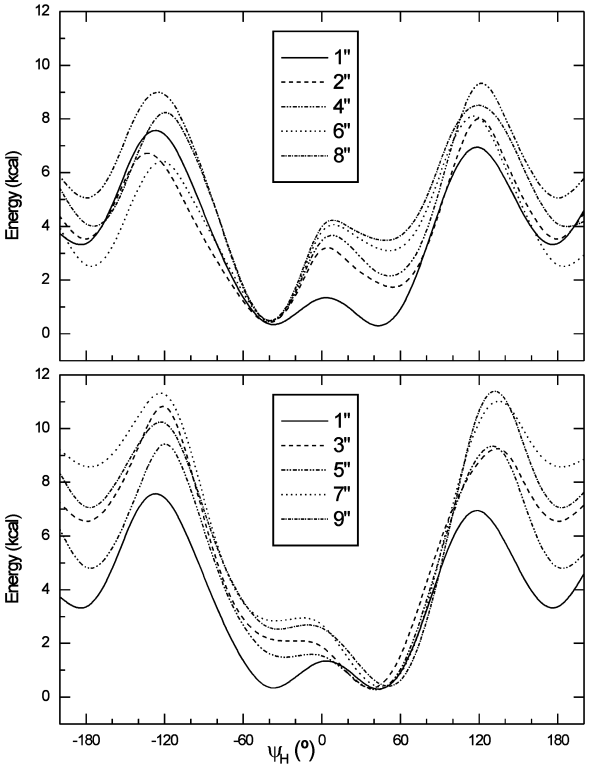

Fig. 5. Relaxed MM3 surface (2D plot) for compounds **1**″–**9**″.

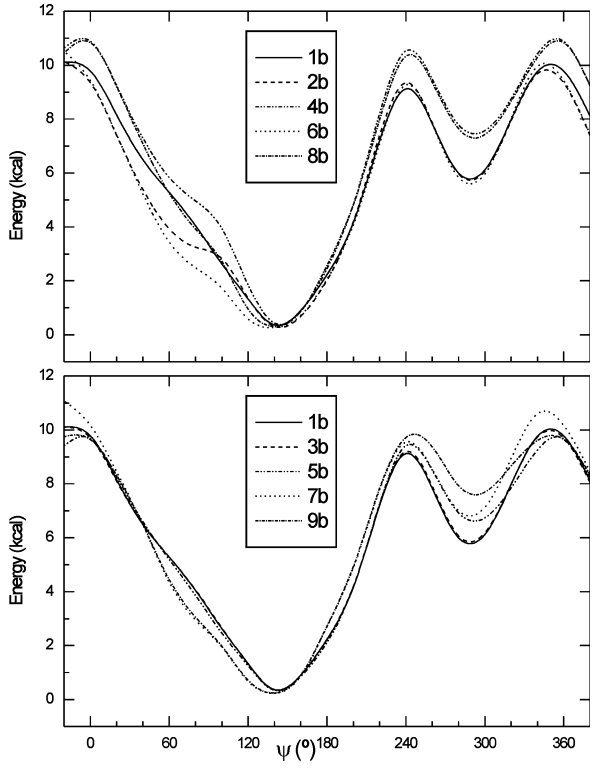

Fig. 6. Relaxed MM3 surface (2D plot) for compounds **1b**–**9b**.

(**1b**) or sulfated on C-4 (**3b**, **5b**, **7b** and **9b**) give much higher values of the ratios (32–35, unshaded triangles on Fig. 8). These facts can be explained on geometrical grounds.

Absolute flexibility. The absolute flexibility Φ[32,33] depends mostly on the geometry and energy of the transition states between minima **A** and **B**, as the other minima usually are higher in energy, and reaching them usually requires high potential barriers.[22,23] In this sense, if the ϕ angle for minimum **A**, minimum **B** and the transition state is exactly the same, the ratio $\Phi_{\phi,\psi}$:Φ_{ψ} should be 0.50, as $(\phi_i - \phi_j)$ becomes zero, and the quotient is 360 instead of 720 (see Section 2). On the other hand, if the average variation of the ϕ angles of the main minima with the transition state has a value similar to the average variation of the ψ angles, the ratio should be 1.0, with the possibility of reaching larger figures if the variation in the ϕ angles is larger than that of the ψ ones, or furthermore, if a low-energy minimum appears outside of the **A**–**B** region, in a region with a sharply different ϕ value. The actual ratio values for more than 80% of the calculated maps is 0.50–0.67 (Tables 2–4, see below for the exceptions), with an average of 0.58, deviating only slightly from the 0.50 value expected theoretically for a map with a fixed

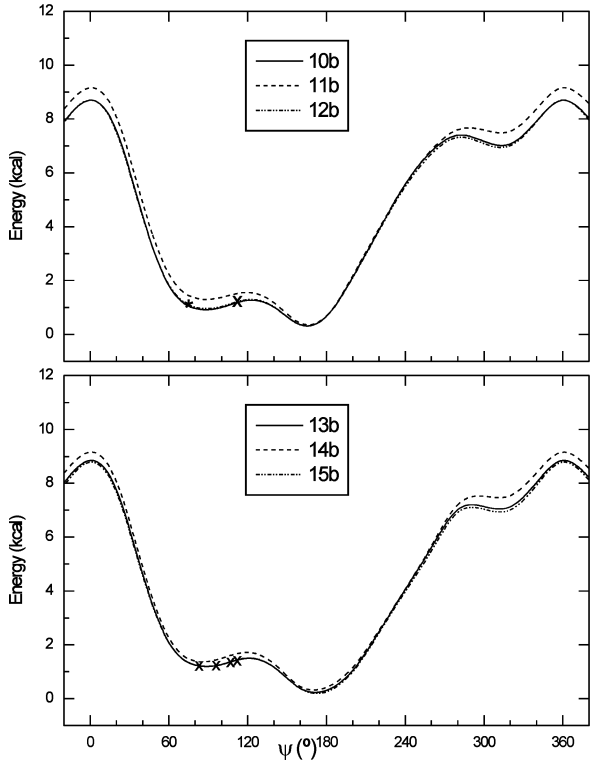

Fig. 7. Relaxed MM3 surface (2D plot) for compounds **10b**–**15b**. The symbols indicate the positions of a published crystal structure[43] related to **10b** (*), and of fiber diffraction studies of carrageenans with repeating units **12b** (×),[39] and **15b** (×).[39–42]

ϕ value. Fig. 9 shows the clear linear correlation obtainable for $\Phi_{\phi,\psi}$ and Φ_{ψ} for compounds **1**–**20**, **1′**–**10′** and **10b**–**15b** (on a logarithmic scale, in order to give less overlapping of points). For disaccharides representing repeating units of carrageenans not carrying 3,6-anhydrogalactose the sulfation pattern of the β-D-galactose unit splits the compounds in two groups, as occurred with the partition function. For α-linked disaccharides, those not sulfated on the β-galactose unit (**1″**) or sulfated on C-4 (**3″**, **5″**, **7″** and **9″**) follow the previously mentioned $\Phi_{\phi,\psi}$:Φ_{ψ} ratio (0.51–0.57, Table 3), while 2-sulfated compounds (**2″**, **4″**, **6″** and **8″**) give much higher values, close to unity (0.91–1.00). The similarity of the Φ values obtained by 3D and 2D measurements for those 2-sulfated compounds can be explained on grounds of geometrical considerations of the minima and the transition state, as shown in Fig. 10. The transition state for **2″** is 'out of the line' determined by **A** and **B**, while the path for **1″** and **3″** is less meandering. These deviations of the $\Phi_{\phi,\psi}$:Φ_{ψ} ratios occur mostly with compounds of low flexibility (as **2″**, **4″**, **6″** and **8″**). The widening of the ϕ low-energy areas can also explain the lack of correlation of the partition functions for these compounds: as low-energy regions extend a little bit more on the ϕ direction, the q_{ψ} yields lower values than those expected when considering the full 3D range. For the corresponding β-linked disaccharides, the $\Phi_{\phi,\psi}$:Φ_{ψ} ratios are higher. However, again, two separate ranges are found: those sulfated on C-2 of the β unit (**2b**, **4b**, **6b** and **8b**) have $\Phi_{\phi,\psi}$:Φ_{ψ} values between 0.71 and 0.89 (Table 4), while the compounds not sulfated (**1b**) or sulfated on C-4 (**3b**, **5b**, **7b** and **9b**) give $\Phi_{\phi,\psi}$:Φ_{ψ} ratios even higher than unity (1.30–1.47, unshaded triangles on Fig. 9). This effect is caused by the geometrical particularities of the **A**–**B** minima, with very close geometries, being closer in their ψ values than in their ϕ values,[23] thus yielding a $\Phi_{\phi,\psi}$:Φ_{ψ} ratio higher than 1.

Concluding remarks. A clear correlation is found between the 3D contour maps (energy as function of ϕ and ψ) and 2D plots (energy as function of ψ) for most of the axially–axially and axially–equatorially linked disaccharides under study. The influence of the sulfation pattern may change the correlation function, but usually the order of flexibilities encountered using ψ as single variable matches those found previously by using both ϕ and ψ as variables.

Conformational features deduced from the 2D plots.— The inspection of the 2D plots (Figs. 1–7) is simpler than that made from the 3D contours. Thus, several conclusions can be rationalized easily with just a rapid look at the maps.

(a) Compounds in which the glycosidic linkage is axial–equatorial (Fig. 1) reach maxima with lower energy than those with an axial–axial linkage (Fig. 2). This has already been measured in terms of the energy

Table 2
Corrected partition functions q and absolute flexibilities Φ, obtained from two- and tri-dimensional plots using the MM3 force field, and ratios between those constants for compounds **1**–**20**[22]

Compd	$\varepsilon = 3$						$\varepsilon = 80$					
	q_ψ (deg)	$q_{\phi,\psi}$ (deg^2)	$q_{\phi,\psi}$:q_ψ	Φ_ψ ($\times 10^4$)	$\Phi_{\phi,\psi}$ ($\times 10^4$)	$\Phi_{\phi,\psi}$:Φ_ψ	q_ψ (deg)	$q_{\phi,\psi}$ (deg^2)	$q_{\phi,\psi}$:q_ψ	Φ_ψ ($\times 10^4$)	$\Phi_{\phi,\psi}$ ($\times 10^4$)	$\Phi_{\phi,\psi}$:Φ_ψ
1	39	960	25	128	82	0.64	79	2180	28	376	210	0.56
2	41	1230	30	24	13	0.54	38	1120	29	60	33	0.56
3	75	2670	36	419	243	0.58	52	1460	28	294	186	0.63
4	45	1530	34	103	57	0.55	55	1570	29	129	73	0.56
5	32	730	22	30	16	0.54	80	2250	28	376	211	0.56
6	57	1430	25	33	18	0.56	40	1180	30	68	38	0.56
7	59	1830	31	142	81	0.57	51	1470	29	292	184	0.63
8	61	1890	31	157	86	0.55	60	1740	29	155	88	0.57
9	52	1650	32	210	105	0.50	43	1220	28	188	116	0.62
10	77	2610	34	636	404	0.63	79	2290	29	550	361	0.66
11	36	850	24	34	19	0.57	32	930	29	40	25	0.61
12	41	1230	30	117	64	0.54	45	1320	29	140	78	0.55
13	67	2010	30	178	113	0.64	44	1340	30	218	134	0.61
14	77	2340	30	570	364	0.64	72	2200	31	528	345	0.65
15	39	1160	30	47	28	0.59	33	1030	31	39	23	0.60
16	52	1560	30	184	104	0.56	51	1560	31	185	103	0.56
17	57	1650	29	133	72	0.54	58	1740	30	133	72	0.54
18	46	1390	30	143	78	0.54	46	1430	31	142	78	0.55
20	56	1770	32	165	94	0.57	58	1970	34	204	119	0.58

Table 3
Corrected partition functions q and absolute flexibilities Φ, obtained from two- and tri-dimensional plots using the MM3 force-field, and ratios between those constants for compounds **1′**–**10′**[21] and **1″**–**9″**[18,20]

Compd	q_ψ (deg)	$q_{\phi,\psi}$ (deg^2)	$q_{\phi,\psi}$:q_ψ	Φ_ψ ($\times 10^4$)	$\Phi_{\phi,\psi}$ ($\times 10^4$)	$\Phi_{\phi,\psi}$:Φ_ψ
1′	80	2140	27	440	258	0.59
2′	79	2100	27	399	226	0.57
3′	41	1040	25	10	6.8	0.65
4′	42	1090	26	15	8.6	0.58
5′	51	1320	26	256	143	0.56
6′	67	1780	26	296	175	0.59
7′	53	1500	28	103	69	0.66
8′	36	780	21	6.4	4.3	0.67
9′	69	2200	32	309	176	0.57
10′	73	2220	30	289	177	0.61
1″	57	1510	26	42	23	0.55
2″	27	870	32	1.9	1.8	0.98
3″	29	570	20	16	8.1	0.51
4″	24	700	29	1.1	1.0	0.94
5″	35	730	21	18	11	0.57
6″	25	870	34	0.6	0.6	1.00
7″	25	530	21	4.6	2.5	0.54
8″	24	850	36	0.45	0.41	0.91
9″	25	590	23	9.5	5.0	0.52

of the **C** minimum,[22] but it also applies to the entire **C** region. However, in the first group, compounds with the reducing unit carrying the D-*galacto* configuration (**2** and **6**) are the highest in their group, while those in the second group carrying the D-*ido* configuration (**12** and **16**) have lower maxima, comparable to those of **2** or **6**.

(b) Minima **A** and **B** appear close in energy for all compounds **1**–**20**. Those with the D-*galacto* configuration show the two minima appear most differentiated, with a considerable energy barrier between them (Fig. 1), as expected from their low flexibility measured by the Φ parameter (Table 2). Most of the other compounds exhibit one of them as the global minimum (usually **B**, but sometimes **A**, especially for compounds with the D-*gluco* configuration)[22] and the other in a flat region in which it is often difficult to determine visually if a minimum is present. However, full-matrix analyses showed they are true minima.[22]

(c) Fig. 3 shows that the cyclic analog with an equatorial-axial 'glycosidic' linkage (**17**) has virtually an

Table 4
Corrected partition functions q and absolute flexibilities Φ obtained from two- and tri-dimensional plots using the MM3 force field, and ratios between those constants for compounds **1b**–**15b**[23]

Compd	q_ψ (deg)	$q_{\phi,\psi}$ (deg^2)	$q_{\phi,\psi}$:q_ψ	Φ_ψ ($\times 10^4$)	$\Phi_{\phi,\psi}$ ($\times 10^4$)	$\Phi_{\phi,\psi}$:Φ_ψ
1b	28	880	32	20	27	1.30
2b	31	860	28	2.6	2.0	0.78
3b	28	890	32	18	25	1.34
4b	26	610	23	0.32	0.28	0.89
5b	29	980	34	24	32	1.33
6b	36	920	26	11	8.1	0.71
7b	35	1140	33	0.76	1.1	1.47
8b	29	660	23	2.1	1.6	0.74
9b	34	1170	35	2.3	3.1	1.36
10b	41	1210	30	113	68	0.60
11b	33	1050	32	71	43	0.61
12b	40	1200	30	109	65	0.60
13b	43	1330	31	75	44	0.58
14b	37	1290	35	55	33	0.60
15b	45	1430	31	74	42	0.56

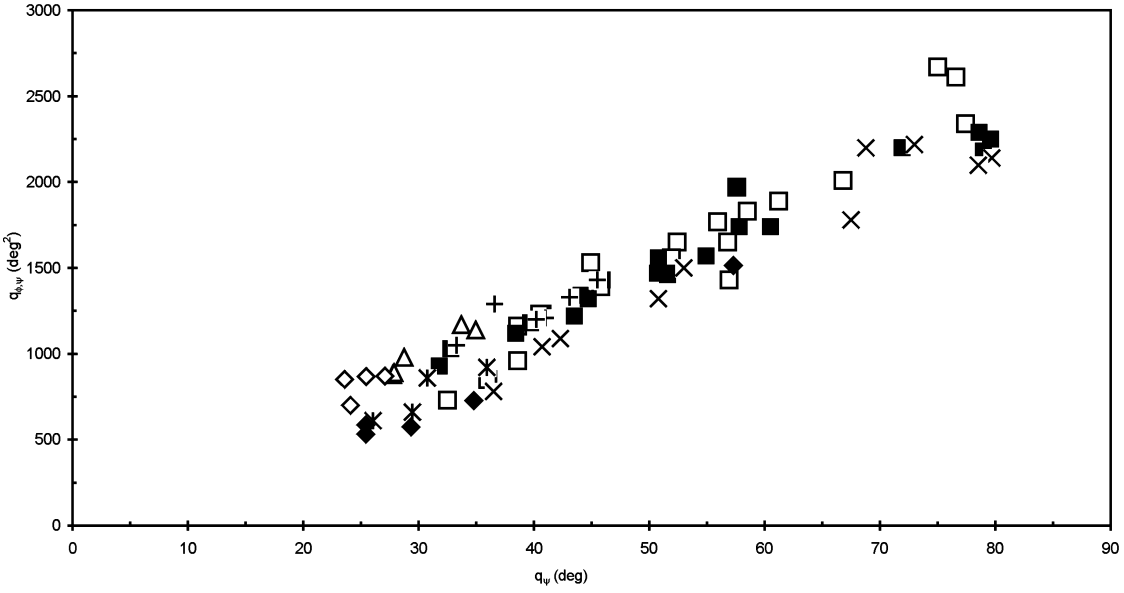

Fig. 8. Relationship between the partition functions $q_{\phi,\psi}$ and q_ψ for compounds **1**–**20** at $\varepsilon = 3$ (■), **1**–**20** at $\varepsilon = 80$ (□), **1′**–**10′** (×), **10b**–**15b** (+), for α-linked disaccharides not sulfated on C-2 **1″**, **3″**, **5″**, **7″** and **9″** (◆), the corresponding 2-sulfated compounds **2″**, **4″**, **6″** and **8″** (◇), and their β-linked equivalents sulfated on C-2 **2b**, **4b**, **6b** and **8b** (✱), and not sulfated on C-2 **1b**, **3b**, **5b**, **7b** and **9b** (△).

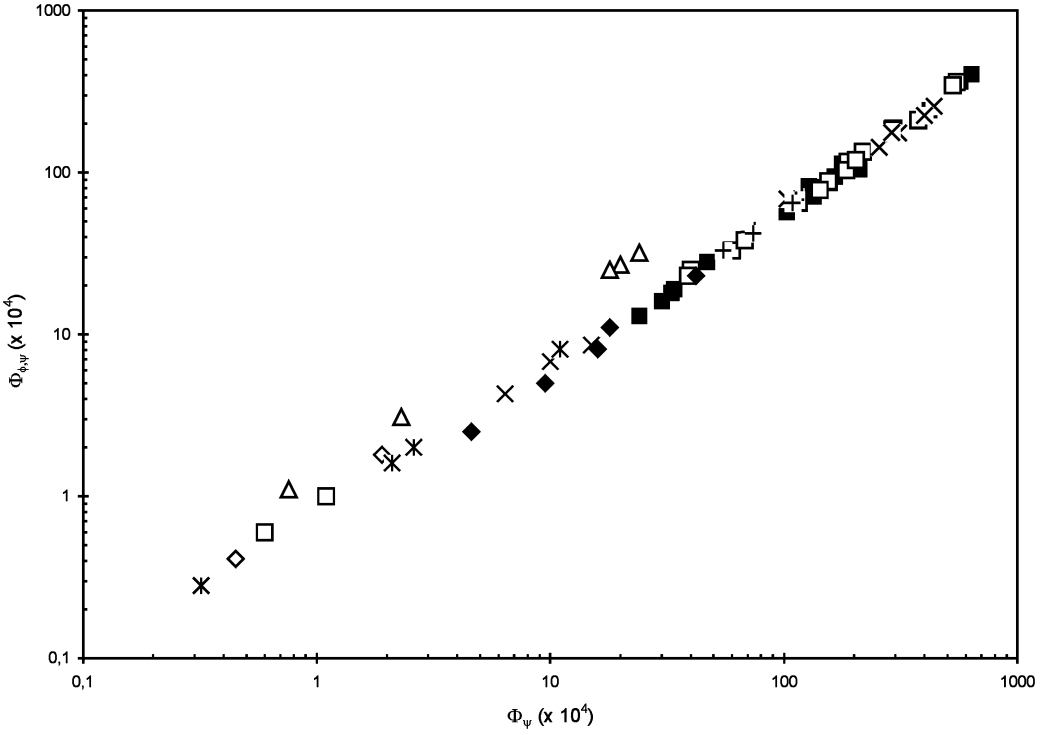

Fig. 9. Relationship between the absolute flexibilities $\Phi_{\phi,\psi}$ and Φ_{ψ} for compounds **1**–**20** at $\varepsilon = 3$ (■), **1**–**20** at $\varepsilon = 80$ (□), **1′**–**10′** (×), **10b**–**15b** (+), for α-linked disaccharides not sulfated on C-2 **1″**, **3″**, **5″**, **7″** and **9″** (◆), the corresponding 2-sulfated compounds **2″**, **4″**, **6″** and **8″** (◇), and their β-linked equivalents sulfated on C-2 **2b**, **4b**, **6b** and **8b** (✳), and not sulfated on C-2 **1b**, **3b**, **5b**, **7b** and **9b** (△).

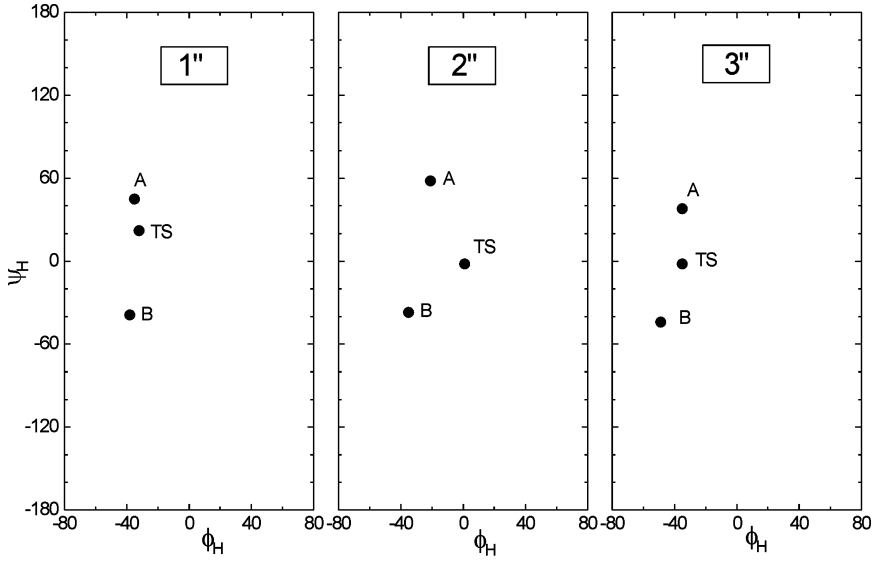

Fig. 10. Diagram representing the location of the **A** and **B** minima, and of the transition state (**TS**) between them on a ϕ,ψ map for compounds **1″**, **2″**, and **3″**.

identical potential energy surface with the acyclic counterpart (**20**), although the latter shows slightly lower energy in the **C** region. The axial–axial tetrahydropyranyl analog (**18**) shows higher relative energies in the **A** and **C** regions, especially the latter.

(d) The influence of sulfation and pyruvylation on the α-(1→3)-linked disaccharide repeating units of carrageenans carrying 3,6-anhydrogalactose is clearly shown in Fig. 4. Very small energy barriers between the **A** and **B** minima are shown to occur (thus explaining their high flexibilities). The compounds that carry a sulfate on position 2 of the β-galactose unit (**3′**, **4′**, **7′**

and **8′**) show a marked increase in the energy of the **A** minima, while a sulfate on C-4 of the same unit (**5′** and **6′**) stabilizes the **A** minima, and the energy in the **C** region is greatly increased. When both sulfates on C-2 and C-4 are present (**7′** and **8′**), the **A**–**B** region is influenced by the effect of the C-2 sulfation, while the **C** region is mostly influenced by the C-4 sulfation. Pyruvylation causes almost no effect (cf. **1′** and **9′**, or **2′** and **10′**), though the **C** region appears somehow changed: pyruvylation decreases the barrier between the **B** and **C** minima, while it increases that between the **A** and the **C** minima.

(e) α-D-Gal*p*-(1→3)-β-D-Gal*p* (**1″**, Fig. 5) exhibits a map with very similar energies in the **A** and **B** regions, with a well-shaped barrier between them. Fig. 5 shows clearly that sulfation on C-2 of the β-unit increases the energy of the **A** minima, thus making **B** the global minimum, while sulfation on C-4 produces exactly an opposite effect. Further sulfation shows a global trend towards stabilizing the **B** minima, in both cases. The sulfate groups on the α-unit have a further influence on the **C** region: for β-galactose 2-sulfated compounds, sulfation on C-2 increases the energy of the **B**–**C** and **A**–**C** barrier regions. For 4-sulfated compounds, the presence of sulfate on C-2 of the α-unit increases the energy of the **C** region, while the presence of 6-sulfate decreases that energy, as previously calculated from the additive effects.[20]

(f) For the disaccharides representing the repeating structures of carrageenans with β-(1→4)-linkages and not carrying 3,6-anhydrogalactose (**1b**–**9b**), only the so-called minimum **A** is observed. Minimum **B** appears at most as a shoulder in the 20° grid (Fig. 6). In the 3D plots the minima were not differentiated.[23] This fact may be rationalized on the basis of a **B** minimum with very little entropy, i.e., geometrically very close to the transition state leading to the **A** minimum. The influence of sulfation is shown to be almost negligible on the plots (Fig. 6), especially for 4-sulfated disaccharides where the **A**–**B** region is almost constant, and only differences in the **C** region can be found due to sulfation on C-2 and/or C-6 of the α-galactose unit. For the β-galactose 2-sulfated products, a larger influence of extra sulfation is shown to occur, mainly increasing the energy of the **C** region (only for 6-sulfate) and changing the shape of the plot close to the **B** region.

(g) When in these disaccharides, α-galactose is replaced by 3,6-anhydrogalactose (**10b**–**15b**, Fig. 7), neat **A** and **B** regions are observed, and the energy of the **C** regions is lowered markedly, as expected considering the change of the linkage from equatorial–axial to equatorial–equatorial.[4,22] Besides, almost no effect of any sulfate groups is shown to occur.[23] Only a slight increase in the energy of the **B** and **C** regions appears by sulfation on C-2 of the β-D-galactose unit.

(h) The reported crystal and fiber structures for the compounds under study[35–43] tend to fall close to region **B** (Figs. 1, 4 and 7). The crystal structures encountered for many disaccharides carry a more or less constant ϕ angle,[27] close to that expected from the *exo*-anomeric effect, as happens with the modeling results. The ψ angle does not vary either very much,[27] with values usually not far from $\psi_H = 0°$, rarely reaching absolute values above 30°. The packing forces present in the crystal are probably forcing the conformation to a position not far from those of the calculated minima, but in any case slightly different from them.

Limitations.—As expected, the possibility of using 2D plots to represent in a simpler fashion entire potential surfaces should be limited to ϕ,ψ surfaces in which a deep trough with a more or less fixed ϕ value appears. Thus, these are certainly not appropriate for trehalose or other non-reducing disaccharides, where there are two ϕ angles and no ψ angle.[16] Besides, other potential energy functions yield sharply different surfaces, with very variable ϕ angles, even for molecules like those shown in the present work.[44,45] Therefore, the procedure is mostly devised for MM3 or other energy functions which yield similar surfaces. Finally, the presence of a perpendicular trough with considerably low energy was shown to appear for equatorially–equatorially linked disaccharides.[15] This second trough leads to a fourth minimum (minimum **D**[21–23]), also called 'side-of-the-map-minimum'.[46] These minima (which also benefit from the *exo*-anomeric effect) carry very high energies for disaccharides with an axial glycosidic linkage,[22,46] but might be more important for disaccharides with an equatorial glycosidic linkage. Although these **D** minima also carried high energy for the equatorially linked neocarrabiose derivatives **1′**–**10′**,[21] relative energies around 3 kcal/mol were found for other β-linked disaccharides (including those studied in the present work),[15,23] leading to scarcely populated structures (usually less than 1%). Furthermore, these energies appear quite higher when considering entropic terms.[21–23] However, further work[46] showed the importance of these minima for low dielectric constants, where strong hydrogen bonds counterweigh the steric hindrance produced by the C-2 substituents. At $\varepsilon = 1.5$, the **D** minima reach 25% of the total population of sophorose and cellobiose populations, while at $\varepsilon = 3.5$ their relative population is around 6%, considering steric energies.[46] In aqueous solution, it has been estimated that this **D** minimum may account for about 10% of the cellobiose population.[47] Even though the presence of such minimum should not be forgotten, 2D plots for these disaccharides should be feasible, as, at least at dielectric constant higher than 1.5, they represent the true adiabatic surface, and account for the most populated regions.

General conclusions.—With the few restrictions signaled above, the 2D plots can represent the potential

energy surfaces of disaccharides as efficiently as 3D contour maps. Their production is much simpler by requiring less computational efforts, and the output is much easier to interpret. Besides, the conversion of a 3D map into a 2D plot leaves the possibility of constructing 3D maps of carbohydrates using a second variable different to ϕ: for instance, the O-5–C-5–C-6–O-6 angle of 6-linked disaccharides[48,49] or even further, a second ψ angle in a trisaccharide (manuscript submitted). Further work in progress on these subjects will throw light on new developments in the representation of the potential energy surfaces of higher saccharides.

Acknowledgements

Both authors are Research Members of the National Research Council of Argentina (CONICET). This work was supported by grants from UBA (X087), Antorchas-Vitae, and CONICET.

References

1. French, A. D.; Brady, J. W. *ACS Symp. Ser.* **1990**, *430*, 1–19.
2. Engelsen, S. B.; Rasmussen, K. *Int. J. Biol. Macromol.* **1993**, *15*, 56–62.
3. French, A. D.; Dowd, M. K. *J. Mol. Struct. (Theochem)* **1993**, *286*, 183–201.
4. French, A. D.; Kelterer, A.-M.; Johnson, G. P.; Dowd, M. K.; Cramer, C. J. *J. Comput. Chem.* **2001**, *22*, 65–78.
5. Melberg, S.; Rasmussen, K. *Carbohydr. Res.* **1979**, *69*, 27–38.
6. Melberg, S.; Rasmussen, K. *Carbohydr. Res.* **1979**, *71*, 25–34.
7. Melberg, S.; Rasmussen, K. *Carbohydr. Res.* **1980**, *78*, 215–224.
8. Tvaroška, I.; Pérez, S. *Carbohydr. Res.* **1986**, *149*, 389–410.
9. French, A. D. *Biopolymers* **1988**, *27*, 1519–1523.
10. Ha, S. N.; Madsen, L. J.; Brady, J. W. *Biopolymers* **1988**, *27*, 1927–1952.
11. French, A. D. *Carbohydr. Res.* **1989**, *188*, 206–211.
12. Tran, V.; Buléon, A.; Imberty, A.; Pérez, S. *Biopolymers* **1989**, *28*, 679–690.
13. Imberty, A.; Tran, V.; Pérez, S. *J. Comput. Chem.* **1989**, *11*, 205–216.
14. Dowd, M. K.; Zeng, J.; French, A. D.; Reilly, P. J. *Carbohydr. Res.* **1992**, *230*, 223–244.
15. Dowd, M. K.; French, A. D.; Reilly, P. J. *Carbohydr. Res.* **1992**, *233*, 15–34.
16. Dowd, M. K.; Reilly, P. J.; French, A. D. *J. Comput. Chem.* **1992**, *13*, 102–114.
17. Dowd, M. K.; French, A. D.; Reilly, P. J. *J. Carbohydr. Chem.* **1995**, *14*, 589–600.
18. Stortz, C. A. *Carbohydr. Res.* **1999**, *322*, 77–86.
19. Stortz, C. A.; Cerezo, A. S. *J. Carbohydr. Chem.* **1994**, *13*, 235–247.
20. Stortz, C. A.; Cerezo, A. S. *J. Carbohydr. Chem.* **1998**, *17*, 1405–1419.
21. Stortz, C. A.; Cerezo, A. S. *J. Carbohydr. Chem.* **2000**, *19*, 1115–1130.
22. Stortz, C. A.; Cerezo, A. S. *J. Carbohydr. Chem.* **2002**, *21*, 355–371.
23. Stortz, C. A. *Carbohydr. Res.*, in press.
24. Stortz, C. A.; Cerezo, A. S. *An. Asoc. Quim. Argent.* **1995**, *83*, 171–181.
25. Goekjian, P. G.; Wu, T.-C.; Kishi, Y. *J. Org. Chem.* **1991**, *56*, 6412–6422.
26. Mikros, E.; Labrinidis, E.; Pérez, S. *J. Carbohydr. Chem.* **2000**, *19*, 1319–1349.
27. Rao, V. S. R.; Qasba, P. K.; Balaji, P. V.; Chandrasekaran, R. *Conformation of Carbohydrates*; Harwood Academic: Amsterdam, 1998; pp 91–130.
28. Allinger, N. L.; Yuh, Y. H.; Lii, J.-H. *J. Am. Chem. Soc.* **1989**, *111*, 8551–8566.
29. Allinger, N. L.; Rahman, M.; Lii, J.-H. *J. Am. Chem. Soc.* **1990**, *112*, 8293–8307.
30. MM3 (96). *Bull. QCPE* **1997**, *17* (1), 3.
31. French, A. D.; Kelterer, A.-M.; Johnson, G. P.; Dowd, M. K.; Cramer, C. J. *J. Mol. Graph. Modelling* **2000**, *18*, 95–107.
32. Lamba, D.; Glover, S.; Mackie, W.; Rashid, A.; Sheldrick, B.; Pérez, S. *Glycobiology* **1994**, *4*, 151–163.
33. Koča, J.; Pérez, S.; Imberty, A. *J. Comput. Chem.* **1995**, *16*, 296–310.
34. Koča, J. *J. Mol. Struct.* **1993**, *291*, 255–269.
35. Neuman, A.; Avenel, D.; Arène, F.; Gillier-Pandraud, H.; Pougny, J.-R.; Sinaÿ, P. *Carbohydr. Res.* **1980**, *80*, 15–24.
36. Luger, P.; Vangehr, K.; Bock, K.; Paulsen, H. *Carbohydr. Res.* **1983**, *117*, 23–38.
37. Warin, V.; Baert, F.; Fouret, R.; Strecker, G.; Spik, G.; Fournet, B.; Montreuil, J. *Carbohydr. Res.* **1979**, *76*, 11–22.
38. Lamba, D.; Segre, A. L.; Glover, S.; Mackie, W.; Sheldrick, B.; Pérez, S. *Carbohydr. Res.* **1990**, *208*, 215–230.
39. Arnott, S.; Scott, W. E.; Rees, D. A.; McNab, C. G. A. *J. Mol. Biol.* **1974**, *90*, 253–267.
40. Millane, R. P.; Nzewi, E. U.; Arnott, S. In *Frontiers in Carbohydrate Research*; Millane, R. P.; BeMiller, J. N.; Chandrasekaran, R., Eds.; Elsevier: London, 1989; pp 104–131.
41. Janaswamy, S.; Chandrasekaran, R. *Carbohydr. Res.* **2001**, *335*, 181–194.
42. Janaswamy, S.; Chandrasekaran, R. *Carbohydr. Res.* **2002**, *337*, 523–535.
43. Lamba, D.; Burden, C.; Mackie, W.; Sheldrick, B. *Carbohydr. Res.* **1986**, *155*, 11–17.
44. Engelsen, S. B.; Rasmussen, K. *J. Carbohydr. Chem.* **1997**, *16*, 773–788.
45. Le Questel, J-Y.; Cros, S.; Mackie, W.; Pérez, S. *Int. J. Biol. Macromol.* **1995**, *17*, 161–175.
46. Mendonca, S.; Johnson, G. P.; French, A. D.; Laine, R. A. *J. Phys. Chem. A* **2002**, *106*, 4115–4124.
47. Stevens, E. S.; Sathyanarayana, B. K. *J. Am. Chem. Soc.* **1989**, *111*, 4149–4154.
48. Brant, D. A.; Liu, H-S.; Zhu, Z. S. *Carbohydr. Res.* **1995**, *278*, 11–26.
49. Dowd, M. K.; Reilly, P. J.; French, A. D. *Biopolymers* **1994**, *34*, 625–638.